Journal of Materials Chemistry B

RSC Publishing

PAPER

View Article Online
View Journal | View Issue

New dextrin nanomagnetogels as contrast agents for magnetic resonance imaging

Cite this: *J. Mater. Chem. B*, 2013, **1**, 5853

C. Gonçalves,[a] Y. Lalatonne,[b] L. Melro,[a] G. Badino,[a] M. F. M. Ferreira,[c] L. David,[d] C. F. G. C. Geraldes,[e] L. Motte,[b] J. A. Martins†[c] and F. M. Gama*[a]

Received 31st July 2013
Accepted 3rd September 2013

DOI: 10.1039/c3tb21063d

www.rsc.org/MaterialsB

This study aims at the production and characterization of a "nanomagnetogel" consisting of superparamagnetic iron oxide nanoparticles (γ-Fe_2O_3) stabilized within a hydrophobized-dextrin nanogel. The nanomagnetogel obtained was extensively characterized with respect to physico-chemical (transmission electron microscopy, cryo-scanning electron microscopy, dynamic light scattering, small angle X-ray scattering), magnetic (relaxometry, MIAplex) and biocompatibility (interaction with cells) properties. The obtained nanomagnetogel formulation, with about 4 mM of iron and a diameter of 100 nm, presents relevant features as a promising magnetic resonance imaging (MRI) contrast agent, noteworthy superparamagnetic behavior, high stability, narrow size distribution and potential for magnetic guidance to target areas by means of an external magnetic field. High values of transverse relaxivity make the nanomagnetogel a promising T_2 contrast agent, allowing enhanced lesion detectability through magnetic resonance imaging. The nanomagnetogel demonstrated non-toxicity for 3T3 fibroblast cultures and was efficiently internalized by bone marrow-derived macrophages, therefore having potential as a contrast agent for MRI of the organs associated with the reticuloendothelial system (spleen, liver). The production of the nanomagnetogel is simple and easy to scale up, thus offering great technological potential.

1. Introduction

Nanotechnology has tremendous potential to contribute towards prevention, diagnosis, imaging, and treatment of several diseases, based on the ability of not only carrying multiple diagnostic/therapeutic payloads in the same package, but also facilitating the targeted delivery into specific sites and across complex biological barriers. In cancer imaging, magnetic resonance imaging (MRI) can offer high spatial resolution and the capacity to simultaneously obtain physiological and anatomical information based on the interaction of contrast agents with the surrounding protons of the tissues.[1] Magnetic nanoparticles (MNPs) exhibit a unique contrast enhancement that enables MRI of cell trafficking, gene expression, and cancer detection.[2–5] In addition, MNPs have been recognized as a promising tool for site-specific delivery of drugs and of diagnostic agents through the application of an external magnetic field.[4,6–11]

Superparamagnetic iron oxide nanoparticles (SPION) are of considerable interest as contrast agents due to their nanoscale dimensions, nontoxic nature and magnetic properties. In medicine, their application in the nude form is limited by their agglomeration in biological fluids, induced by their high surface energies and hydrophobicity, which lead to protein adsorption.[12] Polymer coating provides colloidal stability in water, through steric stabilization, giving well-dispersed formulations. Surface coating of iron nanoparticles with amphiphilic polymers has been described, essentially using synthetic polymers and experimental methodologies relying on organic solvents for phase transfer.[13–15] Such strategies are still limited for their extension to clinical applications, although great efforts have been devoted to the development of simple and effective methods to prepare nanocarriers with high stability and narrow size distributions.

Size[16] and surface properties[17] of nanostructures are particularly important features which strongly affect both the blood circulation time and the bioavailability of the particles within the body. In addition, magnetic properties and internalization depend on the size range.[18] Particles ranging from *circa* 10 to

[a]*IBB-Institute for Biotechnology and Bioengineering, Centre for Biological Engineering, Minho University, Campus de Gualtar, 4710-057, Braga, Portugal. E-mail: fmgama@deb.uminho.pt*

[b]*CSPBAT Laboratory, UMR 7244 CNRS, Université Paris 13, Sorbonne Paris Cité, Bobigny, France*

[c]*Chemistry Department, Minho University, Campus de Gualtar, 4710-057 Braga, Portugal*

[d]*Laboratoire Ingénierie des Matériaux Polymères (IMP@Lyon1) CNRS UMR 5223, Université de Lyon, Université Claude Bernard Lyon 1, 15 boulevard Latarjet, 69622 Villeurbanne Cedex, France*

[e]*Departamento de Ciências da Vida, Faculdade de Ciência e Tecnologia, Centro de, Neurociências e Biologia Celular e Centro de Química, Universidade de Coimbra, Portugal*

† Currently on sabbatical leave at Dep. of Chemistry, University of Bath, UK.

100 nm are small enough to evade the reticuloendothelial system (RES) as well as to penetrate very small capillaries within the body tissues and, therefore, may offer the most effective distribution in certain tissues.[19] The RES, mainly the Kupffer cells in the liver, usually takes up these particles due to their hydrophobic surface and, therefore, results in efficient opsonization.

Currently, two SPION are clinically approved, namely: ferumoxides (Feridex in the USA, Endorem in Europe) and ferucarbotran (Resovist). The SPION effect is observed mainly on T_2^* relaxation and thus MRI is usually performed using T_2/T_2^*-weighted sequences in which the loss of tissue signal is due to the susceptibility effects of the SPION oxide core. Regarding the administration route, Resovist can be administered as a rapid bolus (used with both dynamic and delayed imaging), whereas Feridex needs to be administered by slow infusion (used only in delayed phase imaging). In the liver, these particles are sequestered by phagocytic Kupffer cells in normal tissues, but are not retained in lesions lacking Kupffer cells. Consequently, significant differences in T_2/T_2^* relaxation enhance lesion detectability. Both Feridex and Resovist are approved specifically for MRI of the liver, namely for detection of hepatic metastases. After intravenous administration, clinically approved SPION are cleared from the blood by phagocytosis accomplished in the RES, so that uptake is observed in the normal liver, spleen, bone marrow, and lymph nodes. After the intracellular uptake, SPIONs are metabolized in the lysosomes into a soluble nonsuperparamagnetic form of iron, which becomes part of the iron pool (*e.g.*, ferritin, hemoglobin).[20]

In this study, we aim to develop a novel approach to prepare uniform polymeric particles, by stabilizing iron oxide nanoparticles within dextrin nanogels – a class of nanocarriers well suited for numerous specific delivery applications.[21] Nanogels can be formulated by the self-assembly of amphiphilic polymers. In such a typical self-assembled formulation, the hydrophobic nanodomains formed within a nanogel can be loaded with a variety of therapeutic molecules or imaging agents.[22] Dextrin is an affordable biomaterial, available in large amounts, highly biocompatible, biodegradable and readily excreted through the kidneys due to its fairly low molecular weight. Although already used in the biomedical industry, and available in medical grade, it is clearly underexploited. We aim to develop an effective "nanocarrier" for iron oxide nanoparticles that ensures colloidal stability at physiological pH. The targeted applications are RES organs – as in the case of the aforementioned commercial formulations – or tumor sites, taking advantage of either the enhanced permeation and retention (EPR) effect or active targeting. Therefore, a nanomagnetogel for use as a contrast agent for MRI should exhibit the following properties: (i) high relaxivity, therefore better contrast, minimizing dosage; (ii) size bellow 100 nm, and narrow size distribution, for bolus intravenous administration, instead of slow intravenous infusion; (iii) appropriate coating to allow the magnetic particles to be stable under physiological conditions; (iv) importantly, the coating should be nontoxic and easily cleared from the body.

2. Experimental section

2.1. Materials

Dextrin-VA (dexVA) and dextrin-VA-SC_{16} ($dexC_{16}$) were synthesized as comprehensively described before.[23] DexVA consists of a dextrin backbone with grafted acrylate ester groups (VA—vinyl group). $DexC_{16}$ is composed of the hydrophilic dextrin backbone with grafted VA groups, which are partially substituted with long alkyl chains (SC_{16}). In this work, $dexC_{16}$ with 30 vinyl groups (DS_{VA} 30%) and 4.5 or 14.0 hexadecanethiol chains (DS_{SC16} 4.5 or 14.0%) per 100 dextrin glucopyranoside residues were used. For the sake of simplicity, nanogels containing 4.5 or 14.0% of alkyl chains will be named nanogel 1 (NG1) or nanogel 2 (NG2), respectively.

2.2. Preparation of polymer-coated γ-Fe_2O_3 nanoparticles

The nanogel was obtained by dispersion of $dexC_{16}$ (lyophilized powder) in distilled water, under stirring at 50 °C, until a clear solution was obtained. The dispersion was then filtrated through a 0.22 μm syringe filter. The polymer concentration must be higher than 0.008 mg mL^{-1}, previously identified as the critical micelle concentration (cmc),[23] required for the amphiphilic polymer to self-assemble in water, producing nanostructures internally stabilized through the hydrophobic domains[24] and allowing the solubilization of hydrophobic molecules.[25]

Water-soluble bare γ-Fe_2O_3 nanoparticles were prepared *via* our previously published approach.[26] In a typical synthesis procedure, the first step is to add dimethylamine ($(CH_3)_2NH_2OH$) to an aqueous micellar solution of ferrous dodecyl sulphate ($Fe(DS)_2$). The final concentrations after mixing of the reactants are 1.3×10^{-2} mol L^{-1} and 8.5×10^{-1} mol L^{-1} for $Fe(DS)_2$ and dimethylamine, respectively. The solution is stirred vigorously for 2 h at 28.5 °C and the resulting precipitate of uncoated nanocrystals is isolated from the supernatant by applying a magnetic field. In the second step, this precipitate is washed with a large excess of DI water and redispersed at pH 2.0 leading to stable cationic nanoparticles (zeta = +38 mV and isoelectric point = 7.8).[27]

γ-Fe_2O_3 nanoparticles were loaded into the hydrophobic nanodomains of a dextrin nanogel dispersed in distilled water through hydrophobic–hydrophobic interactions.[28] The physical entrapment of γ-Fe_2O_3 into the nanogel was performed following the nanogel preparation procedure, as described above. A stock solution of γ-Fe_2O_3 (270 mM Fe) was used. The required volume of stock solution was added to the nanogel dispersion and the pH was adjusted to 7.4. The formulation was kept under circular stirring overnight to allow γ-Fe_2O_3 incorporation into the nanogel, through hydrophobic/hydrophobic interactions. After that, formulations were centrifuged at 4000*g* for 10 min (room temperature), to remove non-stabilized γ-Fe_2O_3. The supernatant was carefully collected and analyzed.

The effect of the nanogel/γ-Fe_2O_3 ratio on the loading efficiency and stability of the formulation was studied. Different nanogel@γ-Fe_2O_3 formulations were prepared, using distilled water as the dispersion medium, by varying the iron

concentration (1.4, 5.0, 10.0 mM) and the polymer concentration (1.0 or 2.0 mg mL^{-1}). In order to evaluate the stability of the dispersions, they were maintained at 4 °C up to 8 weeks as described below.

2.3. Physico-chemical characterization of polymer-coated γ-Fe_2O_3 nanoparticles (nanogel@γ-Fe_2O_3)

2.3.1. γ-Fe_2O_3 loading. The iron quantification was carried out by atomic absorption spectroscopy (AAS) (GBC 932 Plus, PerkinElmer). The instrument response was periodically checked using appropriate standard solutions. Formulations were stored at 4 °C until measurement.

2.3.2. Size distribution and colloidal stability. The formulation stability was evaluated by analysing the nanogel size distribution, up to 8 weeks, keeping the formulation at 4 °C. The size distribution was determined by dynamic light scattering (DLS) using a Malvern Zetasizer, model Nano ZS (Malvern Instruments Limited, UK). The nanogel dispersion was analysed at 25 °C in a polystyrene cell, using a He–Ne laser – a wavelength of 633 nm and a detector angle of 173°. The DLS analysis provides the characterization of a sample through the mean value (*z*-average) for the diameter, and a width parameter known as the polydispersity index (PdI).

2.3.3. Microscopy: cryo-SEM and TEM. For Cryo-SEM analysis, nanogel@γ-Fe_2O_3 formulations were rapidly immersed in liquid nitrogen slush at −95 °C for 2 min and vacuum transferred to an Alto 2500 (Gatan Inc., CA) cryo preparation chamber attached to a JEOL JSM 6301F scanning electron microscope. Frozen samples were fractured at −95 °C, etched for 10 seconds (to partially sublime water from the fractured nanogel surface), and finally gold-coated for 2 min. Samples were viewed at −50 °C and the resulting SEM images were analyzed using ImageJ software (National Institute of Health, USA).

Transmission electron microscopy (TEM) micrographs were obtained using a JEOL 2010 TEM instrument at an accelerating voltage of 160 kV. Samples were prepared by wetting carbon-coated grids with a small drop of colloidal dispersions.

2.3.4. SAXS experiment. The SAXS experiment was carried out at the European Synchrotron Radiation Facility (Grenoble, France) on the BM2-D2AM beamline. The suspensions were installed in silica tubes (external diameter of 3 mm, wall thickness of 0.2 mm, 76 mm long, from Deutero GmbH, ref. 2000942) with elastomer closure caps to avoid water evaporation (Deutero ref. 29 604 15). The incident photon energy was set to 16.000 keV to limit attenuation by the glass tubes. We used a 2D CCD X-ray detector from Roper Scientific. The images were corrected for camera distortion, dark image reading and the flat field response of the detector. Finally, the image center ("gravity center" of the incident beam) was determined with attenuators and radial averages yielded 1D profiles (processing carried on the beamline, with bm2img software). The angle or *q*-calibration was performed thanks to a silver behenate powder standard placed in a glass tube in the 21-sample holder. The subtraction of the scattering contribution of the empty cell (glass tube filled with water) was performed by measuring the attenuation coefficient of the samples. A dextrin nanogel (NG1 or NG2) was dispersed in distilled water.

2.3.5. Magnetic properties

2.3.5.1. Relaxometry. Magnetic resonance relaxometry was used to measure the longitudinal (T_1) and transverse (T_2) proton relaxation times for the nanogel@γ-Fe_2O_3 formulations. Measurements were performed using a Bruker Minispec mq20 relaxometer operating at a magnetic field of 0.47 T, corresponding to a Larmor frequency of 20 MHz, and at a temperature of 25 °C. T_1 and T_2 relaxation times were obtained using the inversion-recovery (IR) and Carr–Purcell–Meiboom–Gill (CPMG) pulse sequences, respectively. The reproducibility of the relaxation time determinations was found to be better than ±1%. The corresponding relaxivity values, r_1 and r_2, were calculated through the least-squares curve fitting of 1/relaxation time R_i ($i = 1,2$) (s^{-1}) *versus* the iron concentration (mM Fe).

2.3.5.2. MIAplex assay. In the MIAplex® (Multiplex Magnetic Immuno Assays) instrument, a magnetic material is exposed simultaneously to two alternative magnetic fields, a magnetic field of low frequency $f_1 = 0.025$ Hz and a magnetic field of higher frequency $f_2 = 24.4$ kHz. During MIAplex® measurements, the amplitude of the high frequency magnetic field (f_2) is fixed at a value lying between −8.88 Oe and 8.88 Oe, while the amplitude of the low frequency magnetic field (f_1) is varied between −452.4 Oe and 452.4 Oe. A signal, which is proportional to the second derivative of the magnetization curve of the material, d^2M/dH^2, is then recorded, at room temperature, when the amplitude of the high frequency magnetic field is varied.[29]

2.4. *In vitro* studies

2.4.1. Nanomagnetogel guidance and stability under an external magnetic field. Magnetic nanoparticles loaded into a nanogel offer the possibility of magnetically guiding the formulations. To understand the nanomagnetogel responsiveness/stability under a magnetic field, an *in vitro* study was performed. Nanogel@γ-Fe_2O_3 formulation, using NG1 (2.0 mg mL^{-1}) and 5.0 mM of initial iron concentration was prepared, as previously described. An Eppendorf tube containing the nanomagnetogel dispersion was placed next to a magnet overnight, allowing the accumulation of the nanomagnetogel particles next to the magnet. Then, the supernatant was collected without removing the magnet and the total volume was replaced with freshly distilled water; finally, the magnet was removed and the accumulated pellet was redispersed. The samples "before magnet", "after magnet" and "redispersed" were analyzed by atomic absorption spectroscopy for iron quantification. Each sample was also analyzed by Fourier transform infrared spectroscopy (FTIR), after lyophilisation, to ascertain whether the nanogel co-localizes with iron oxide, during magnetic field application.

For FTIR analysis, KBr tablets of each sample were prepared by mixing 2.5 mg of the sample with KBr (total mixture mass of 250 mg). The mixture was ground until a homogeneous and fine powder was obtained. The material was pressed using a hydraulic press, for *ca.* 3 min, to form the tablet. The tablet was

gently taken out of the mold and kept at 60 °C overnight, before analysis, to make sure that samples were properly dried. The tablet should be translucent; otherwise, the spectrum may have low-resolution, since little infrared radiation passes through the sample. A background reading was performed before sample analysis in a FTIR spectrophotometer (Nicolet 380 FTIR Thermo Electro Corporation).

2.4.2. Cell cultures

2.4.2.1. Mouse embryo fibroblasts 3T3 culture. Mouse embryo fibroblasts 3T3 (ATCC CCL-164) were grown in Dulbecco's modified Eagle's medium supplemented with 10% newborn calf serum (Invitrogen, CA) and 1% penicillin/streptavidin (DMEM complete medium [cDMEM]) at 37 °C in 95% humidified air containing 5% CO_2.

2.4.2.2. Murine bone marrow-derived macrophages (BMDM). Macrophages were obtained from mouse bone marrow as follows: mice were sacrificed and femurs and tibias removed under aseptic conditions. Bones were flushed with Hank's balanced salt solution. The resulting cell suspension was centrifuged at 500 × *g* for 10 min and resuspended in RPMI 1640 medium supplemented with 10 mM HEPES, 10% heat-inactivated fetal bovine serum (FBS), 60 μg mL^{-1} penicillin/streptavidin, 0.005 mM β-mercaptoethanol (complete RPMI [cRPMI]), and 10% L929 cell conditioned medium. To remove fibroblasts or differentiated macrophages, cells were cultured on cell culture dishes (Sarstedt, Canada), overnight at 37 °C in a 5% CO_2 atmosphere. Then, non-adherent cells were collected with warm cRPMI and centrifuged at 500 × *g* for 10 min. Cells were distributed on 24-well plates (Sarstedt, Canada) at a density of 5×10^5 cells per well (1 mL) and incubated at 37 °C in a 5% CO_2 atmosphere. Four days after seeding, 10% of L929 cell conditioned medium was added, and the medium was renewed on the seventh day. After ten days in culture, cells were completely differentiated into macrophages. This method allows for the differentiation of a homogeneous primary culture of macrophages that retain the morphological, physiological and surface marker characteristics of these phagocytic cells.[30,31]

2.4.3. Cell interaction studies

2.4.3.1. Cell viability – MTT assay. The viability of mouse embryo fibroblast 3T3 cells, after incubation with nanogel or nanogel@γ-Fe_2O_3 formulations, was evaluated, *in vitro*, using the 3-(4,5-dimethylthiazol-2-yl)-2,5-diphenyltetrazolium bromide (MTT) assay. The tetrazolium salt is widely used to quantify cell viability, by colorimetry. In this test, the tetrazolium salt is metabolically reduced to highly colored end products, formazans.[32] The succinate-tetrazolium reductase system, which belongs to the mitochondrial respiratory chain, is active only in viable cells. The measured absorbance (at 570 nm) is proportional to the global metabolic activity that is hypothesized to be proportional to the number of viable cells. For each sample, the background optical density (evaluated at a wavelength of 690 nm) was subtracted; the test was performed in triplicate for each condition.

A negative control experiment was performed using cells without any treatment (growing in culture medium). Nanogel or nanogel@γ-Fe_2O_3 formulations, using NG1 or NG2, were incubated with cells, for 24 or 48 h. The MTT assay was performed at the beginning (0 h) to check the absorbance of cell cultures, in order to investigate the cell growth during the assay. Each formulation was diluted in the culture medium using different dilution factors (DF), DF5 and DF10. These values are based on the assumption that, when using a mouse model, the injection of 200 μL on the blood circulation (whose total volume is around 1500 μL) would result in a dilution factor of 7.5. The nanogel concentrations tested are 0.4 mg mL^{-1} and 0.2 mg mL^{-1} in the DF5 and DF10 conditions, respectively.

MTT was added, at each time point, to the culture medium with a final concentration of 0.5 mg mL^{-1}. After 3 h of incubation, the insoluble formazan crystals were solubilized with DMSO, and the absorbance was measured at 570 and 690 nm using an automated ELISA plate reader.

2.4.3.2. Phagocytic activity – Prussian blue. In order to evaluate the phagocytic activity, murine bone marrow derived macrophages (5.0×10^5 cells per well) were seeded on coverslips and exposed to the nanogel (NG1) 0.4 mg mL^{-1}, as the negative control, or NG1@γ-Fe_2O_3 formulation (nanogel 0.4 mg mL^{-1}; iron 0.8 mM) for 3 h. The cover glasses were washed twice with PBS aiming to remove the excess iron. After that, the iron content of the cells was assessed using the Prussian blue staining procedure (5% potassium ferrocyanide and 5% HCl mixed 1 : 1 for 30 min). Cover glasses were analysed using an inverted light microscope (Leica DM IL).

3. Results and discussion

3.1. Characterization of polymer-coated γ-Fe_2O_3 nanoparticles (nanogel@γ-Fe_2O_3)

3.1.1. γ-Fe_2O_3 loading. The coating of SPION with amphiphilic polymers is a suitable strategy to achieve colloidal stability of iron oxide in water through steric stabilization. Self-assembled hydrogel nanoparticles (nanogel) from amphiphilic polymers provide an interesting architecture wherein the hydrophobic nanodomains serve as suitable carriers for hydrophobic iron oxide nanoparticles; the hydrophilic polymeric matrix allows for particle stabilization in aqueous solution (Scheme 1).

The stabilization of γ-Fe_2O_3 nanoparticles within a dextrin nanogel was studied, using different iron concentrations (1.4, 5.0 or 10.0 mM) added to a nanogel concentration of 1.0 or 2.0 mg mL^{-1}. Each formulation was prepared using NG1

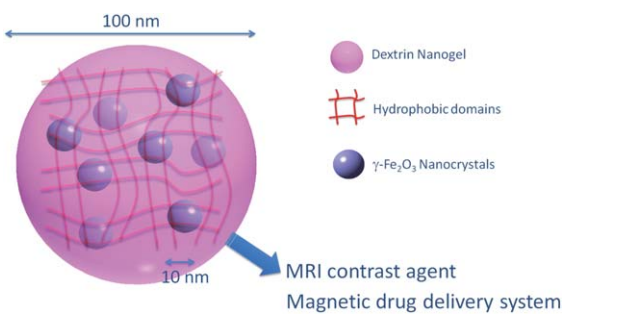

Scheme 1 Schematic of a nanomagnetogel for use as an MRI contrast agent and drug delivery system.

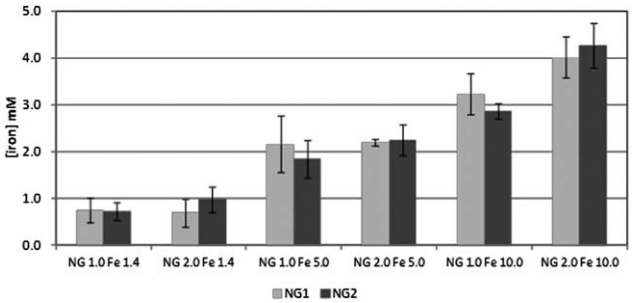

Fig. 1 Iron concentration (mM) effectively stabilized (incorporated within the nanogel) after the addition of different iron concentrations (1.4, 5.0 or 10.0 mM) within 1.0 or 2.0 mg mL^{-1} of NG1 (▒) or NG2 (■), as determined by atomic absorption spectroscopy. Results represent the mean ± S.D. of at least 2 independent assays.

(DS_{SC16} 4.5%) and NG2 (DS_{SC16} 14.0%), so as to understand the impact of the dextrin degree of substitution on the loading capacity. After the mixture, pH was adjusted to 7.4 and formulations were incubated overnight, at room temperature. After incubation, non-stabilized γ-Fe_2O_3 was removed through centrifugation (4000*g*, 10 min). The concentration of stabilized γ-Fe_2O_3 (supernatant) was determined by atomic absorption spectroscopy (Fig. 1).

Concerning the influence of the dextrin degree of substitution with hydrophobic chains, only a minor difference in the loading capacity was observed comparing NG1 (DS_{SC16} 4.5%) and NG2 (DS_{SC16} 14.0%). Therefore, we only used NG1 since it contains less hydrophobic chains and no significant benefit results from using a higher DS_{C16}.

An increase in nanogel concentration (from 1.0 to 2.0 mg mL^{-1}) does not result in significantly higher loadings, when lower initial iron concentrations were used. When a higher initial iron concentration was used (10 mM), a slight increase in iron incorporation was observed for the higher nanogel concentration. Since even higher nanogel concentrations are not possible, since 2.0 mg mL^{-1} is already close to the solubility limit, a nanomagnetogel with NG1 2.0 mg mL^{-1} and 10.0 mM of initial iron concentration was selected as the most promising one, which corresponds to a formulation with about 4.0 mM of iron.

3.1.2. Size distribution, zeta potential and colloidal stability. Modified dextrin self-assembles in water, producing a nanogel with a bimodal size distribution with two populations

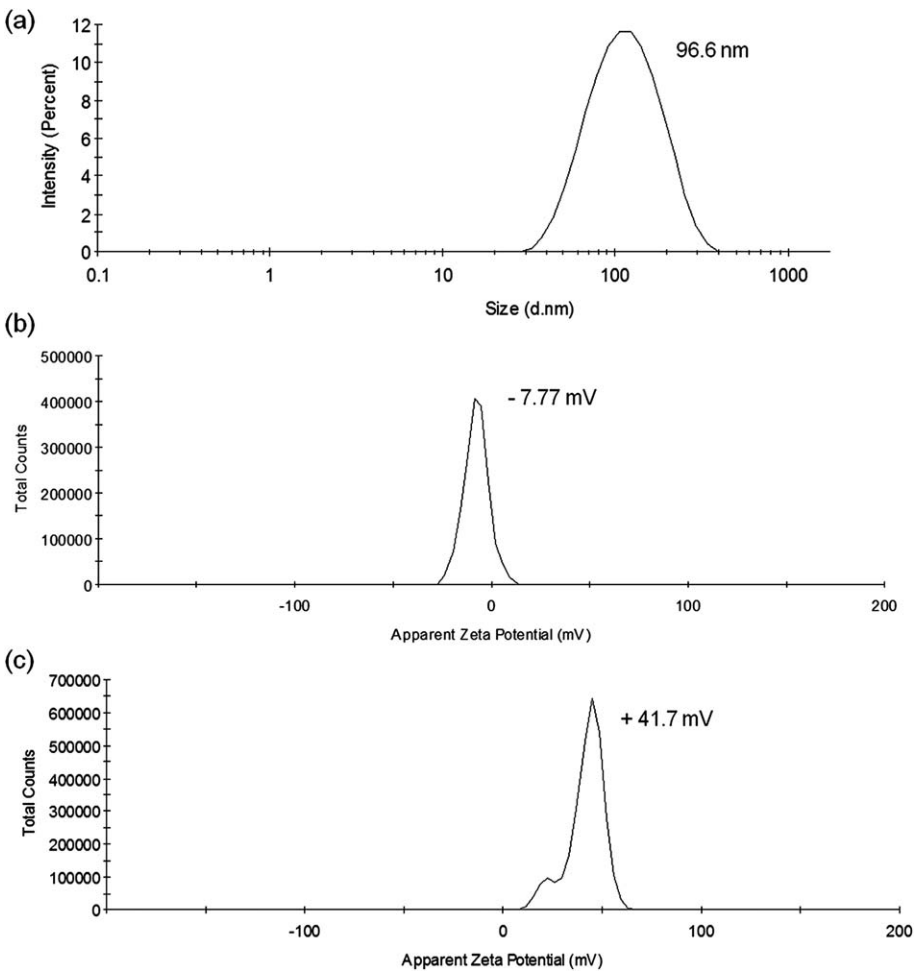

Fig. 2 Size distribution in intensity (a) and zeta potential of nanogel@γ-Fe_2O_3 (NG1 2.0 mg mL^{-1} loaded with 4.0 mM Fe) at pH 7.4 (b) and zeta potential of bare γ-Fe_2O_3 nanoparticles, 4.0 mM Fe at pH 2.0 (c).

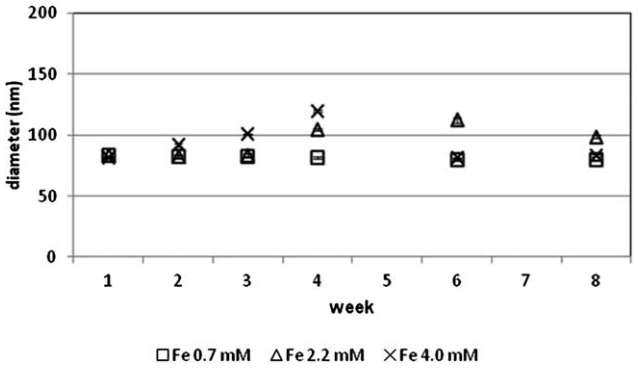

Fig. 3 Size evaluation (diameter, nm) of different nanogel@γ-Fe_2O_3 formulations (pH 7.4) using NG1 2.0 mg mL^{-1} loaded with 0.7 (□), 2.2 (Δ) or 4.0 (×) mM of iron, up to 8 weeks. Results represent the mean ± S.D. of 5 consecutive measurements.

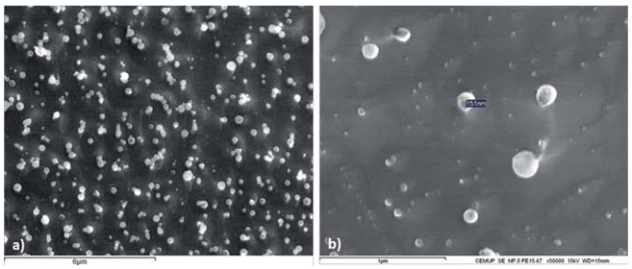

Fig. 4 Cryo-SEM images of nanogel@γ-Fe_2O_3 formulations: (a) NG1 2.0 mg mL^{-1}, iron concentration of 2.2 mM, 10 000×; and (b) NG1 1.0 mg mL^{-1}, iron concentration of 2.2 mM, 50 000×.

with diameters 20 and 100 nm, as shown previously.[33] Remarkably, after γ-Fe_2O_3 addition, the size distribution profile exhibits a single peak and an average diameter around 100 nm (Fig. 2a).

The nanomagnetogel shows a zeta potential value close to zero (−7.77 mV) (Fig. 2b), as previously reported for the dextrin nanoparticles without iron (−5.0 mV).[24] Bare γ-Fe_2O_3 nanoparticles present a large positive zeta potential value, 41.7 mV (Fig. 2c). The zeta potential value demonstrates that the iron oxide particles are internalized within the nanogel, such that the nanomagnetogel has a near neutral surface charge. Similar results were obtained for the encapsulation of magnetic nanoparticles into liposomes.[34]

The stability of different nanogel@γ-Fe_2O_3 formulations in water was evaluated by analysing the size distribution (intensity-weighted diameter), up to 8 weeks. As can be seen in Fig. 3, the size distribution is almost the same for all formulations studied (80–120 nm) and the hydrodynamic size (diameter) is constant up to 8 weeks of storage (4 °C).

The results suggest that the formulations obtained may have satisfactory shelf stability, although longer assays (up to one year) must still be carried out.

3.1.3. Microscopy: cryo-SEM and TEM. In order to visualize the size distribution and the shape of the nanomagnetogel, nanogel@γ-Fe_2O_3 formulations were visualized by cryo-SEM and TEM.

As can be seen in Fig. 4, the nanomagnetogel has a spherical shape and the size distribution is in good agreement with the previously presented DLS results. Scanning electron microscopy is not suited to reveal the presence of core iron nanoparticles. For this purpose, formulations were also visualized by transmission electron microscopy. This technique allows the visualization of iron oxide nanoparticles as dark spots. TEM images present a clear difference in nanoparticle organization depending on the presence or absence of the nanogel (Fig. 5). A uniform deposition on the TEM grid is observed for bare γ-Fe_2O_3 nanoparticles prepared under acidic conditions (Fig. 5a).

Fig. 5b and c show γ-Fe_2O_3 clusters that must be stabilized by the nanogel; otherwise, the iron oxide would precipitate at pH 7.4. Indeed, the as-synthesized nanoparticles present an isoelectric point (IEP) of 7.8.[27] The TEM images demonstrate that the nanomagnetogel comprises magnetic iron oxide nanoparticles randomly distributed within the polymer structure. Due to a low polymer contrast, the dextrin corona cannot be seen in the TEM images. The nanomagnetogel size is not affected by the degree of substitution of the polymer, since similar results were obtained for NG1 (Fig. 5b) and NG2 (Fig. 5c).

3.1.4. SAXS analysis of dextrin nanogel. The internal nanostructure of iron-free nanogels (NG1 and NG2) was studied by small angle X-ray scattering (SAXS), in a convergent approach with the electron microscopy study of the nanomagnetogel

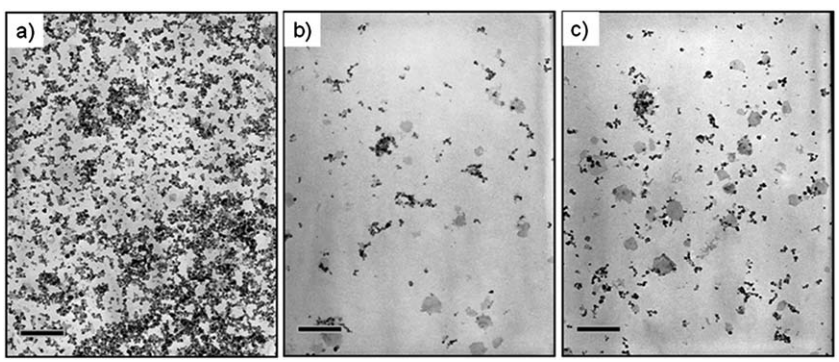

Fig. 5 TEM images of bare γ-Fe_2O_3 nanoparticles (a) and nanogel@γ-Fe_2O_3 formulations using 2.0 mg mL^{-1} nanogel: (b) NG1 iron concentration of 2.0 mM and (c) NG2 iron concentration of 2.2 mM (scale bar 200 nm).

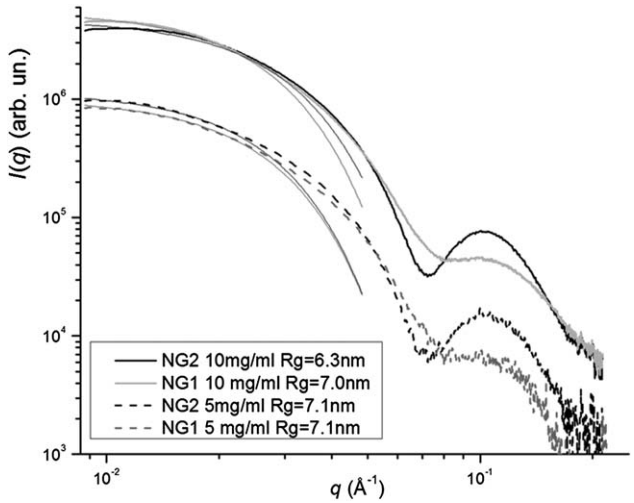

Fig. 6 SAXS analysis of NG1 and NG2 at 5.0 and 10.0 mg mL^{-1}.

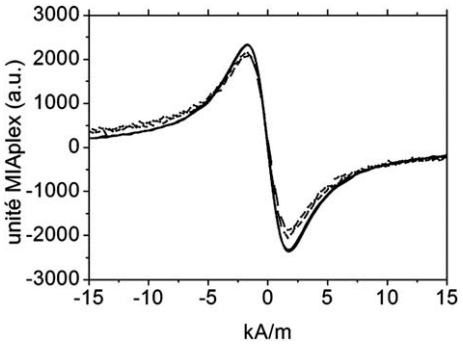

Fig. 7 MIAplex® signal of the nanogel@γ-Fe_2O_3 formulation Fe = 1.4 mM (dotted line) compared to bare γ-Fe_2O_3 nanoparticles (full line).

presented above. The SAXS analysis reveals the nanoscaled organization of hydrophobic domains within the nanogel structure. The scattering patterns shown in Fig. 6 for NG1 and NG2 at two different concentrations are typical of micellar organizations with the gyration radius between 6.3 and 7.1 nm (diameter about 13–15 nm) and a form factor maximum in the q-range from 0.1 to 0.15 Å. The scattering pattern is thus due to the micellar organization within the nanogels and yields the gyration radius of the micelles. The number of hydrophobic domains within the nanogel was previously reported and depends on the degree of substitution of the polymer used: it varies from 15 to 22 for DS_{C16} 4.5 and 10.0%, respectively.[24] The hydrophobic nanodomain sizes obtained here are compatible with such estimations. As shown in Fig. 6, the intraparticular sizes of nanodomains within the nanogels are weakly affected by the degree of substitution of the polymer, since similar results were obtained for NG1 and NG2.

Iron oxide nanoparticles, mostly in the 10–20 nm size range, were visualized by electron microscopy (Fig. 5) and organized in small clusters in the presence of nanogels. Such nanoparticles are known to be stabilized in the hydrophobic core of polymer micelles.[15] Therefore, we can assume that the main driving force for the internalization of iron nanoparticles within the nanogels is due to the hydrophobic interactions between iron oxide nanoparticles and the hydrophobic domains since they exhibit sizes (above 10 nm diameter) compatible with the internalization of an individual iron oxide nanoparticle. Thus, the hydrophobic domains may play a key role in the internalization of iron oxide particles. Further studies are necessary to conclude if the hydrophobic domain structure is affected by the presence of γ-Fe_2O_3 particles, and which hydrophobic domain nanostructure is the most suited for iron oxide nanoparticle internalization (number of hydrophobic nanodomains per nanogel, aggregation number in hydrophobic nanodomains, *etc.*).[24]

3.1.5. Magnetic properties. Numerous experimental and clinical studies have shown that the use of high relaxivity contrast agents results in improved detection and delineation of tumors allowing a more reliable diagnostic.[1] SPIONs have been clinically used as T_2-type (negative) MRI contrast agents.[35,36] Superparamagnetic behavior means that the nanoparticles are highly magnetized in a magnetic field but lose their magnetization when the field is switched off. This behavior is important for injectable formulations, because it reduces the risk of thrombosis from magnetically aggregated nanoparticles. Increasing SPION size can increase its transverse relaxivity.[37] However, the large particles (with sizes approximately larger than 15 nm) are not superparamagnetic and easily aggregate in solution.[28] A strategy to increase T_2 relaxivity, while keeping the superparamagnetic characteristics, is clustering individual SPIONs into clusters, within a polymeric structure such as, in this work, dextrin, which determines their physical parameters, such as the apparent hydrodynamic diameter and surface charge.

The as-synthesized nanocrystals exhibit superparamagnetic behavior at room temperature and do not present remanence as well on magnetization as a second derivative of the magnetization curve. The magnetic properties of nanomagnetogel formulations were investigated with a MIAplex magnetometer at room temperature. The second derivative of the magnetization curves obtained for the nanomagnetogel is not modified compared to bare nanoparticles (Fig. 7). No hysteresis loops appear and this result indicates that the nanogel formulation preserves its superparamagnetic behavior.[38]

The performance of different nanogel@γ-Fe_2O_3 formulations as potential MRI contrast agents was evaluated based on relaxometric measurements. The relaxation times (T_i), the water proton relaxation rate enhancements ($R_i = 1/T_i$) per mM Fe concentration and relaxivities (r_i) ($i = 1$ for longitudinal or $i = 2$ for transverse) are good *in vitro* indicators of their efficiency as positive or negative MRI contrast agents. The inverse relaxation times, R_i, vary linearly with the Fe concentration, according to eqn (1)

$$R_{1,2} = r_{1,2}\,[\mathrm{Fe}] + R_{1,2}{}^{0} \quad (1)$$

where $R_{1,2}{}^{0}$ are the inverse relaxation times in pure water.

As presented above, nanogel@γ-Fe_2O_3 formulations were prepared, and depending on the nanogel concentration and on the amount of iron added, different amounts of iron can be stabilized within hydrophobic nanodomains. r_1 and r_2 values

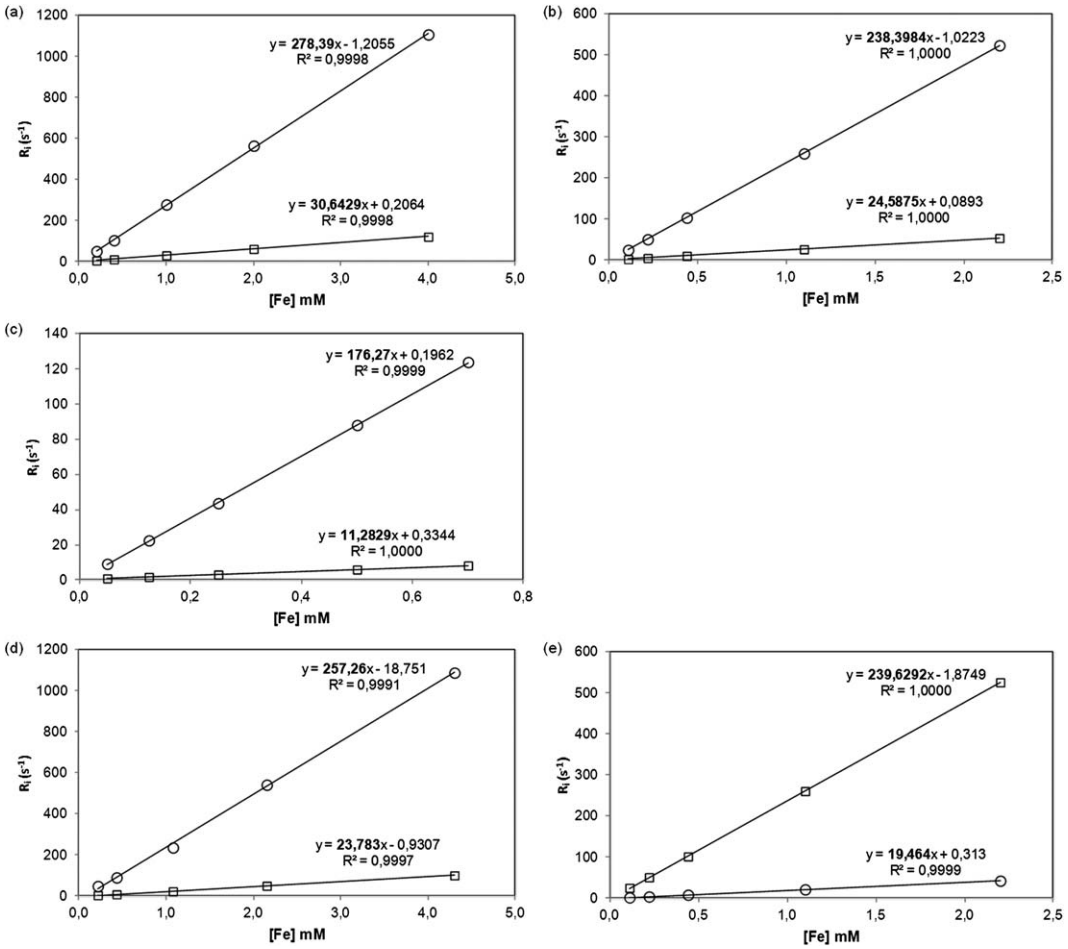

Fig. 8 Longitudinal (□) and transverse (○) relaxivities of nanogel@γ-Fe_2O_3 formulations using 2.0 mg mL^{-1} NG1 loaded with (a) 4.0, (b) 2.2 and (c) 0.7 mM of iron or 2.0 mg mL^{-1} NG2 loaded with (d) 4.3 and (e) 2.2 mM of iron, plotted against iron concentration (dilution assay).

were obtained, after the graphic representation of eqn (1), for different nanogel@γ-Fe_2O_3 formulations using NG1 or NG2 (Fig. 8). Therefore, each formulation was diluted and the relaxation time was measured at five different iron concentrations. r_1 and r_2 values obtained for each formulation are presented in Table 1. As can be seen, r_1 values vary from 11.3 up to 30.6 mM^{-1} s^{-1} and r_2 from 176.3 mM^{-1} s^{-1} up to 278.4 mM^{-1} s^{-1}. Similar transverse relaxivities were obtained using NG1 or NG2. Regarding longitudinal relaxivities, NG1 displays a slight increase when compared to NG2. For both nanogels, an increase in iron content results in higher values of relaxivity. An effect that can be explained by increased dipolar interactions which result from the increase of γ-Fe_2O_3 nanoparticles into the nanogel and leading to higher r_2 values.[39]

Previous studies indicate that clustering magnetic nanoparticles result in enhanced transverse relaxivity. Berret *et al.* fabricated a maghemite nanocluster and tuned the size of aggregates in the 70–150 nm range with aggregation numbers (number of nanoparticles per aggregate) from tens to hundreds. It was found that r_2 was noticeably increased with the size of the magnetic clusters.[40] Ai *et al.* had also obtained a similar result for magnetic nanoparticles encapsulated into the hydrophobic cores of 20–100 nm polymeric micelles.[41]

Ferumoxides and ferucarbotran are commercial SPIONs coated with low molecular weight dextran and carboxydextran, respectively. Regarding the particle size, Feridex is 72 nm[42] and Resovist is 65 nm[43] in diameters. Table 1 shows longitudinal (r_1) and transverse (r_2) relaxivities of NG1 or NG2 formulations, prepared in this work, in comparison with the values of commercial products.

Nanogel@γ-Fe_2O_3 formulations are promising as T_2 contrast agents due to the larger r_2 value. It appears that formulations developed in this study exhibit superior relaxivity properties than those commercially available. Nanomagnetogels loaded with the highest iron content (around 4.0 mM) present high potential as contrast agents for MRI, as shown in Table 1.

3.2. *In vitro* studies

3.2.1. Nanomagnetogel accumulation by an external magnetic field. The entrapment of magnetic nanoparticles inside a nanogel leads to the formation of a nanomagnetogel which may be magnetically driven under an external magnetic field. We have observed this response by placing (overnight) a magnet next to an Eppendorf tube containing the nanomagnetogel dispersion.

Table 1 Values of longitudinal (r_1) and transverse (r_2) relaxivities of NG1 or NG2 (2.0 mg mL^{-1}) formulations compared with commercial products obtained from the literature (values at 0.47 T, 20 MHz)

Material	r_1 (mM^{-1} s^{-1})	r_2 (mM^{-1} s^{-1})
Ferumoxides (Feridex, AMI-25, Endorem)[42]	40	160
Ferucarbotran (Resovist)[43]	25	177
NG1Fe 4.0 mM	31 ± 0.3	278 ± 2.3
NG1Fe 2.2 mM	25 ± 0.1	238 ± 0.3
NG1Fe 0.7 mM	11 ± 0.04	176 ± 0.9
NG2Fe 4.3 mM	24 ± 0.2	257 ± 4.5
NG2Fe 2.2 mM	20 ± 0.1	240 ± 0.7

Fig. 9 Demonstration of nanomagnetogel accumulation under an external magnetic field (overnight).

As shown in Fig. 9, the nanomagnetogel was attracted by the magnetic field and concentrated on the Eppendorf wall, next to the magnet. We aimed at understanding whether the magnetic field application induces nanomagnetogel accumulation or only iron NP accumulation, due to putative disassembly of the nanomagnetogel. Three samples were taken for qualitative (FTIR) and quantitative (atomic absorption spectroscopy) evaluation: before magnetic field application, supernatant after magnetic field application (without removing the magnet) and redispersed material in fresh water (after magnet remotion).

Atomic absorption spectroscopy reveals that the initial colloidal nanomagnetogel suspension has 2.2 mM of iron ("before magnet"), which is halved to 1.1 mM of iron, after the application of the magnetic field ("after magnet"); after magnet removal, the material dispersion leads to 0.8 mM of iron in the "redispersed" sample.

Fig. 10a shows the nanogel FTIR spectra, where the carbonyl group band appears at 1723 cm^{-1} and other dextrin bands appear at 1635, 1408, 1296, 1192 and 1023 cm^{-1}.[44] Otherwise,

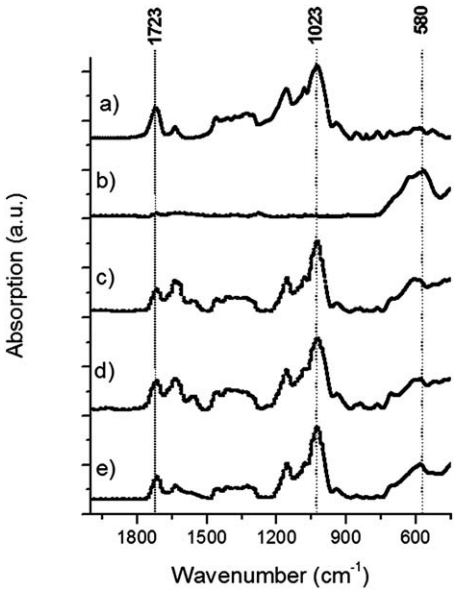

Fig. 10 FTIR spectra of (a) nanogel, (b) bare γ-Fe_2O_3, (c) nanomagnetogel before magnet application, (d) sample after magnet application and (e) redispersed material resulting from magnet application.

γ-Fe_2O_3 (Fig. 10b) reveals a single peak in the FTIR spectrum at 580 cm^{-1}.[45] Before magnet application, the FTIR spectrum of the nanomagnetogel contains peaks assigned to the nanogel and γ-Fe_2O_3 (Fig. 10c). FTIR results demonstrate that, after magnetic field application, part of the nanomagnetogel remains dispersed in the supernatant fraction (Fig. 10d). In order to increase the nanomagnetogel accumulation, longer periods of time or a stronger magnet should be applied. On the other hand, the fraction retained due to magnetic field application contains both iron and the nanogel, as can be verified from Fig. 10e ("redispersed material"). This experiment demonstrates the possibility of magnetically guiding the nanomagnetogel to the targeted area through application of an external magnetic field, without compromising the nanomagnetogel integrity.

3.2.2. Cell viability – MTT assay. In the cell interaction studies, nanogel@γ-Fe_2O_3 formulations were tested using NG1 or NG2, up to 48 h of incubation with mouse embryo fibroblast 3T3 cells. A negative control experiment was performed using cells without any treatment; the influence of the "empty nanogel" (without an iron core) on the cell's viability was also evaluated. Each formulation – 2.0 mg mL^{-1} of the nanogel loaded with 4.0 mM (NG1) or 4.3 mM (NG2) of iron – was diluted in the culture medium 5 or 10 fold resulting in nanogel concentrations of 0.4 mg mL^{-1} and 0.2 mg mL^{-1}, respectively. Bare γ-Fe_2O_3 nanoparticles could not be tested due to their precipitation in the culture medium.

It is assumed that in the MTT assay the absorbance of MTT crystals is proportional to the number of viable cells. The absorbance was determined just before addition of the nanogel or nanomagnetogel formulations (0 h) and after incubation for 24 or 48 h. Both NG1 and NG2 samples were tested to ascertain whether the degree of substitution with hydrophobic chains

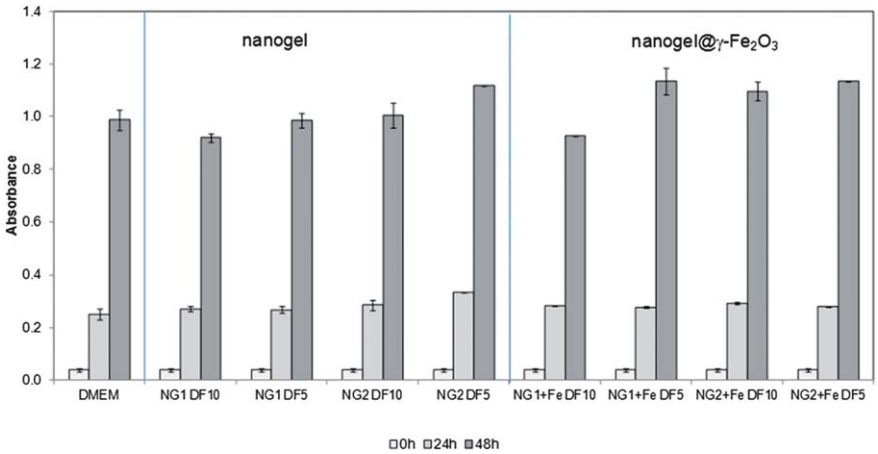

Fig. 11 Cell proliferation assay, in mouse embryo fibroblast 3T3 cells, after 0, 24 or 48 h of incubation in culture medium (DMEM), with nanogel (NG1 or NG2) or nanogel@γ-Fe_2O_3 formulations, using different dilution factors (DF). Results represent the mean ± S.D. of 3 absorbance values obtained from triplicates of each condition.

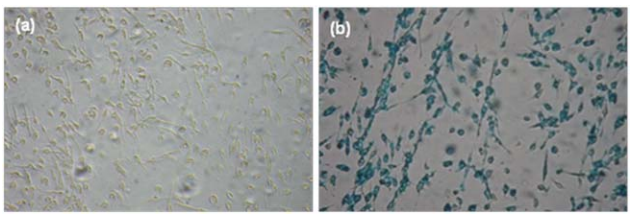

Fig. 12 Uptake of (a) nanogel (NG1) 0.4 mg mL^{-1} or (b) NG1@γ-Fe_2O_3 (nanogel 0.4 mg mL^{-1} and iron 0.8 mM), by murine bone marrow derived macrophages (BMDM), 3 h after incubation staining with Prussian blue (original magnification 100×).

affects cell proliferation. As shown in Fig. 11, cells treated with either nanogels present similar absorbance to the control (untreated cells). Therefore, the nanogel has no significant effect on cell proliferation, independent of the degree of substitution or concentrations used. The same conclusion emerges for nanogel@γ-Fe_2O_3 formulations, indicating that the presence of iron loaded into the nanogel does not affect the proliferation of 3T3 fibroblasts. Therefore, it may be concluded that the dextrin nanomagnetogel is not cytotoxic.

3.2.3. Phagocytic activity – Prussian blue. The mechanism of the cellular uptake of nanoparticles and their biodistribution depend on the physico-chemical properties of the particles and in particular on their surface characteristics. Moreover, as particles are mainly recognized and engulfed by immune cells, special attention should be paid to nano-immuno interactions. It is also important to use primary cells for testing the biocompatibility of nanoparticles, as they are closer to the *in vivo* situation when compared to transformed cell lines.[46]

Fig. 12 shows the efficient uptake of the nanomagnetogel by BMDMs. The cells were stained with Prussian blue to detect the intracellular iron content. The negative control (Fig. 12a) did not show any blue staining. When cells are incubated with the nanomagnetogel (Fig. 12b), the blue colour is clearly visible within cells, revealing the nanomagnetogel internalization by macrophages, 3 h after *in vitro* incubation. Therefore, it can be assumed that the studied formulations are expected to be internalized by phagocytic cells, namely macrophages, after *in vivo* administration, resulting in spleen and liver accumulation. In this way, the formulations developed in this study present great potential as contrast agents for RES rich organs (spleen, liver). Future work intends to use a PEG-decorated nanomagnetogel aiming to escape the phagocytic system and target different organs. Additional molecules can be used for active targeting on the nanomagnetogel surface.

4. Conclusions

In this study, we have shown that the nanomagnetogel production is simple, reproducible, and exhibits long-term colloidal stability (in water dispersions), at least up to 8 weeks. Our first goal was to explore nanogel loading efficacy, using different nanogel/γ-Fe_2O_3 ratios and nanogels with different degrees of substitution with alkyl chains (hydrophobic part). The inner structure of the nanomagnetogel was elucidated by combining dynamic light scattering, transmission electron microscopy and small-angle X-ray scattering analysis.

The nanomagnetogel has a diameter of around 100 nm and comprises superparamagnetic nanoparticles randomly distributed within the polymer structure. The surrounding corona of dextrin allows iron oxide stabilization avoiding aggregation at physiological pH. The nanogel with the lowest degree of substitution with alkyl chains (NG1) 2.0 mg mL^{-1} and 10.0 mM of initial iron concentration was selected as the most interesting formulation, which corresponds to a nanomagnetogel with about 4.0 mM iron content. Incorporation of iron oxide within the nanogel structure results in promising relaxometric properties, essentially as a T_2 contrast agent for MRI. Our nanomagnetogel exhibits superior r_2 values to commercially available formulations.

The nanomagnetogel formulations offer the possibility of magnetic accumulation, through an external magnetic field, to a targeted area, without compromising the nanomagnetogel integrity. The efficient internalization of the nanomagnetogel

by BMDM leads to the inference that, after intravenous administration, formulations will certainly be internalized by phagocytic cells, resulting in the accumulation in RES rich organs (spleen, liver). The nanogel and nanomagnetogel demonstrate no cytotoxic effect on 3T3 fibroblast cultures, up to 48 h of incubation.

Acknowledgements

The authors thank the Magnisense Corporation for providing a MIAplex reader and CFGCG the EU COST TD1004 Action "Theragnostics Imaging and Therapy". The authors thank Prof Cidália Botelho for the iron analysis by atomic absorbance spectroscopy at the Oporto University – Chemical Engineering Department. C. Gonçalves, J. A. Martins and M. F. M. Ferreira acknowledge FCT Portugal, for post-doc grant SFRH/BPD/70524/2010, sabbatical grant SFRH/BSAB/1328/2013 and PhD grant SFRH/BD/63994/2009, respectively.

References

1 A. S. Merbach, L. Helm and E. Tóth, in *The chemistry of Contrast Agents in Medical Magnetic Resonance Imaging*, John Wiley & Sons Inc, 2nd edn, 2013.
2 B. F. Pan, D. X. Cui, Y. Sheng, C. G. Ozkan, F. Gao, R. He, Q. Li, P. Xu and T. Huang, *Cancer Res.*, 2007, **67**, 8156.
3 F. Q. Hu, L. Wei, Z. Zhou, Y. L. Ran, Z. Li and M. Y. Gao, *Adv. Mater.*, 2006, **18**, 2553.
4 S. Chen, L. Wang, S. L. Duce, S. Brown, S. Lee, A. Melzer, A. Cuschieri and P. Andre, *J. Am. Chem. Soc.*, 2010, **132**, 15022.
5 Y. Lalatonne, M. Monteil, H. Jouni, J. M. Serfaty, O. Sainte-Catherine, N. Lievre, S. Kusmia, P. Weinmann, M. Lecouvey and L. Motte, *J. Osteoporosis*, 2010, **2010**, 747852.
6 Y. Sun, Z. L. Chen, X. X. Yang, P. Huang, X. P. Zhou and X. X. Du, *Nanotechnology*, 2009, **20**, 135102.
7 G. Gao, P. Huang, Y. X. Zhang, K. Wang, W. Qin and D. X. Cui, *CrystEngComm*, 2011, **13**, 1782.
8 Z. L. Chen, Y. Sun, P. Huang, X. X. Yang and X. P. Zhou, *Nanoscale Res. Lett.*, 2009, **4**, 400.
9 J. R. McCarthy, K. A. Kelly, E. Y. Sun and R. Weissleder, *Nanomedicine*, 2007, **2**, 153.
10 F. Geinguenaud, I. Souissi, R. Fagard, L. Motte and Y. Lalatonne, *Nanomedicine: Nanotechnology, Biology and Medicine*, 2012, **8**, 1106.
11 L. Motte, F. Benyettou, B. C. de, M. Lecouvey, I. Milesovic and Y. Lalatonne, *Faraday Discuss.*, 2011, **149**, 211.
12 J. Park, M. K. Yu, Y. Y. Jeong, J. W. Kim, K. Lee, V. N. Phan and S. Jon, *J. Mater. Chem.*, 2009, **19**, 6412.
13 D. Kim, M. K. Yu, T. S. Lee, J. J. Park, Y. Y. Jeong and S. Jon, *Nanotechnology*, 2011, **22**, 155101.
14 C. A. J. Lin, R. A. Sperling, J. K. Li, T. Y. Yang, P. Y. Li, M. Zanella, W. H. Chang and W. G. J. Parak, *Small*, 2008, **4**, 334.
15 N. Nasongkla, E. Bey, J. M. Ren, H. Ai, C. Khemtong, J. S. Guthi, S. F. Chin, A. D. Sherry, D. A. Boothman and J. M. Gao, *Nano Lett.*, 2006, **6**, 2427.
16 G. Sonavane, K. Tomoda and K. Makino, *Colloids Surf., B*, 2008, **66**, 274.
17 F. Esmaeili, M. H. Ghahremani, B. Esmaeili, M. R. Khoshayand, F. Atyabi and R. Dinarvand, *Int. J. Pharm.*, 2008, **349**, 249.
18 L. H. Bu, J. Xie, K. Chen, J. Huang, Z. P. Aguilar, A. Wang, K. W. Sun, M. S. Chua, S. So, Z. Cheng, H. S. Eden, B. Z. Shen and X. Y. Chen, *Contrast Media Mol. Imaging*, 2012, **7**, 363.
19 G. Storm, S. O. Belliot, T. Daemen and D. D. Lasic, *Adv. Drug Delivery Rev.*, 1995, **17**, 31.
20 Y. X. Wang, *Quant. Imaging Med. Surg.*, 2011, **1**, 35.
21 R. H. Fang and L. Zhang, *J. Nanoeng. Nanomanuf.*, 2011, **1**, 106.
22 D. Peer, J. M. Karp, S. Hong, O. C. FaroKHzad, R. Margalit and R. Langer, *Nat. Nanotechnol.*, 2007, **2**, 751.
23 C. Gonçalves, J. A. Martins and F. M. Gama, *Biomacromolecules*, 2007, **8**, 392.
24 C. Gonçalves and F. M. Gama, *Eur. Polym. J.*, 2008, **44**, 3529.
25 C. Gonçalves, P. Pereira, P. Schellenberg, P. J. Coutinho and F. M. Gama, *J. Biomater. Nanobiotechnol.*, 2012, **3**, 178.
26 Y. Lalatonne, C. Paris, J. M. Serfaty, P. Weinmann, M. Lecouvey and L. Motte, *Chem. Commun.*, 2008, 2553.
27 F. Benyettou, Y. Lalatonne, I. Chebbi, B. M. Di, J. M. Serfaty, M. Lecouvey and L. Motte, *Phys. Chem. Chem. Phys.*, 2011, **13**, 10020.
28 X. A. Xie and C. F. Zhang, *J. Nanomater.*, 2011, **2011**, 152524.
29 Y. Lalatonne, F. Benyettou, D. Bonnin, N. Lièvre, P. Monod, M. Lecouvey, P. Weinmann and L. Motte, *J. Magn. Magn. Mater.*, 2009, **321**, 1653.
30 R. J. Tushinski, I. T. Oliver, L. J. Guilbert, P. W. Tynan, J. R. Warner and E. R. Stanley, *Cell*, 1982, **28**, 71.
31 X. Zhang, R. Goncalves and D. M. Mosser, *Curr. Protoc. Immunol.*, 2008, ch. 14, unit 14.1, pp. 1–18.
32 T. Mosmann, *J. Immunol. Methods*, 1983, **65**, 55.
33 C. Goncalves, E. Torrado, T. Martins, P. Pereira, J. Pedrosa and F. M. Gama, *Colloids Surf., B*, 2010, **75**, 483.
34 F. Benyettou, I. Chebbi, L. Motte and O. Seksek, *J. Mater. Chem.*, 2011, **21**, 4813.
35 C. F. G. C. Geraldes and S. Laurent, *Contrast Media Mol. Imaging*, 2009, **4**, 1.
36 S. Laurent, D. Forge, M. Port, A. Roch, C. Robic, L. V. Elst and R. N. Muller, *Chem. Rev.*, 2008, **108**, 2064.
37 M. R. J. Carroll, R. C. Woodward, M. J. House, W. Y. Teoh, R. Amal, T. L. Hanley and T. G. St Pierre, *Nanotechnology*, 2010, **21**, 35103.
38 M. C. de, Y. Lalatonne, D. Bonnin, N. Lievre, M. Lecouvey, P. Monod, V. Russier and L. Motte, *Small*, 2012, **8**, 1945.
39 N. C. Bigall, C. Wilhelm, M. L. Beoutis, M. Garcia-Hernandez, A. A. Khan, C. Giannini, A. Sanchez-Ferrer, R. Mezzenga, M. E. Materia, M. A. Garcia, F. Gazeau, A. M. Bittner, L. Manna and T. Pellegrino, *Chem. Mater.*, 2013, **25**, 1055.
40 J. F. Berret, N. Schonbeck, F. Gazeau, D. El Kharrat, O. Sandre, A. Vacher and M. Airiau, *J. Am. Chem. Soc.*, 2006, **128**, 1755.

41 H. Ai, C. Flask, B. Weinberg, X. Shuai, M. D. Pagel, D. Farrell, J. Duerk and J. M. Gao, *Adv. Mater.*, 2005, **17**, 1949.
42 L. Josephson, J. Lewis, P. Jacobs, P. F. Hahn and D. D. Stark, *Magn. Reson. Imaging*, 1988, **6**, 647.
43 J. Qin, S. Laurent, Y. S. Jo, A. Roch, M. Mikhaylova, Z. M. Bhujwalla, R. N. Muller and M. Muhammed, *Adv. Mater.*, 2007, **19**, 1874.
44 H. Garcia, A. S. Barros, C. Gonçalves, F. M. Gama and A. M. Gil, *Eur. Polym. J.*, 2008, **44**, 2318.
45 I. Milosevic, H. Jouni, C. David, F. Warmont, D. Bonnin and L. Motte, *J. Phys. Chem. C*, 2011, **115**, 18999.
46 A. Kunzmann, B. Andersson, T. Thurnherr, H. Krug, A. Scheynius and B. Fadeel, *Biochim. Biophys. Acta, Gen. Subj.*, 2011, **1810**, 361.